Marine mineral-catalyzed NO and N_2O formation on the anoxic early Earth

S. Buessecker,[1§]* H. Imanaka,[2,3] T. Ely,[4] R. Hu,[5,6] S.J. Romaniello,[4,7] H. Cadillo-Quiroz[1,8]*

[1] School of Life Sciences, Arizona State University, Tempe, AZ, USA.
[2] SETI Institute, Mountain View, CA, USA.
[3] NASA Ames Research Center, Moffett Field, CA, USA.
[4] School of Earth and Space Exploration, Arizona State University, Tempe, AZ, USA.
[5] Jet Propulsion Laboratory, California Institute of Technology, Pasadena, CA, USA.
[6] Division of Geological and Planetary Sciences, California Institute of Technology, Pasadena, CA, USA.
[7] Department of Earth and Planetary Sciences, University of Tennessee, Knoxville, TN, USA.
[8] Biodesign Institute, Arizona State University, Tempe, AZ, USA.

§ Current address: Department of Earth System Science, Stanford University, Stanford, CA, USA.
* Correspondence to: S. Buessecker (sbuessecker@stanford.edu), H. Cadillo-Quiroz (hinsby@asu.edu)

Abstract

Microbial metabolisms were limited by available terminal electron acceptors in the anoxic environment of the early Archean. However, iron mineral phases in Fe^{2+}-rich (ferruginous) oceans could have catalyzed reactions with abiotically fixed nitrogen leading to the formation of nitrous oxide (N_2O), a potentially favorable terminal electron acceptor. We experimentally simulated anoxic surface-catalyzed reduction of nitrite and nitrate via green rust and magnetite. Besides N_2O, we detected and quantified the formation of substantial amounts of nitric oxide (NO). While N_2O escaped into the gas phase (63% of nitrite-nitrogen, with green rust as catalyst), NO remained associated with precipitates (7% of nitrite-nitrogen). Using diffusion and photochemical modeling, we show that marine N_2O emissions could have sustained atmospheric N_2O pools of 1-7 ppb. Although this concentration was insufficient to cause significant warming, the seawater enriched in N_2O and NO could have critically affected early benthic life by providing the opportunity to conserve energy.

Introduction

The Archean atmosphere prior to the Great Oxidation Event (GOE) was likely dominated by N_2 and CO_2, with ppm-levels of CO, CH_4, and H_2 (*1*). The introduction of even trace amounts of more oxidized gases, such as nitrous oxide (N_2O), or laughing gas, would have created a significant source of thermodynamic disequilibrium to drive early Archean ecosystems. Microbial N_2O consumption is based on high-affinity enzymes that are adapted to low N_2O steady-state concentrations (*2*). For example, 30 nM N_2O was readily metabolized in anoxic seawater from modern oxygen minimum zones (*3*), but the critical N_2O threshold for marine N_2O respiration is probably much lower (*2*).

Despite the proposed key role of N_2O in the early stages of the Earth's biosphere (*4*, *5*) and climate under a faint young Sun (*6*), it is unknown whether the ocean acted as a net N_2O source to the atmosphere prior to ~2.7 Ga. While earlier estimates of atmospheric N_2O abundances were based on biological production rates (*7*, *8*), more recently, abiotic sources of N_2O have been considered on the early Earth (*5*, *9*). Stanton *et al.* first showed through experiments and modeling that aqueous Fe^{2+} could have acted as a driver for chemodenitrification to form N_2O abiotically in Proterozoic oceans (*5*). Multiple lines of evidence suggest that the oceans were extensively rich in Fe^{2+} (ferruginous) from >3.8 to ~2.7 Ga and had a tendency to export reduced species to the atmosphere (*10*). The ferrous-ferric hydroxy salt carbonate green rust (GR, $[Fe^{2+}_{(1-x)} Fe^{3+}_{x} (OH)_2]^{x+} \cdot [(x/2)CO_3^{2-} \cdot (m/2)H_2O]^{x-}$) has been shown to precipitate from Archean seawater-analog solutions, consistent with thermodynamic modeling predicting a predominance of GR in the Fe sink fraction along the water column (*11*). It has been argued that settling GR particles could have provided a transport mechanism for trace compounds to the seafloor (*11*), where reducing conditions converted GR to magnetite (Fe_3O_4), which is an important constituent of banded iron formations. Nitrogen oxides are prone to become spontaneously reduced in presence of iron mineral phases (*12*, *13*). As a consequence of abiotic nitrogen fixation, nitrite (NO_2^-) and nitrate (NO_3^-) reached seawater concentrations in the lower µM range (*14-17*). Geochemical reactions that consume dissolved NO_x^- species on early Earth include reduction to ammonia (*18*) and reduction of NO_3^-, NO_2^- and N_2 during water-rock interactions between hydrothermal fluids and the oceanic crust (*19*, *20*). However, NO_x^- conversion to ammonia is not significant at $pH \leq 7.3$ (*18*), a regime that dominated the early oceans (*21*), and therefore restricted this NO_x^- sink to more alkaline environments such as ultramafic-hosted hydrothermal vents. In light of the NO_x^- reduction catalyzing potential of GR and magnetite, the question arises as to whether their precipitation in ferruginous seawater could have driven abiotic reactions that form N_2O at rates above the photochemical destruction rate. As the major sink for N_2O is atmospheric photolysis to form N_2, such reactions could complete a fully abiotic denitrification from NO_x^- to N_2, hundreds of millions of years prior to the biological and more efficient production of N_2O (*22*).

Here, we evaluated the role of Archean abiotic N_2O formation, including intermediary NO cycling, from NO_x^- compounds using microcosm experiments that mimic ferruginous seawater conditions. We used the mixed-valence iron minerals GR and magnetite as catalysts for the reduction of NO_2^- and NO_3^- at *low* (1-5 µM), *high* (20-35 µM), and *excessive* (200-350 µM) abundances, and a simple end-member artificial seawater recipe with a 20% CO_2-HCO_3^- buffer devoid of sulfur. These experiments, together with diffusive and photochemical models, allowed us to estimate NO and N_2O abundances in the ocean-atmosphere system of the Archean.

Results and Discussion

Iron mineral reactions with nitrate and nitrite under simulated Archean ocean conditions. We first compared the reactivity of NO_2^- and NO_3^- with GR, magnetite and aqueous Fe^{2+} separately. For all reductants, consumption of NO_3^- and N_2O production was negligible (< 0.03 nmol h^{-1}, Fig. 1A) even over a prolonged period of 100 days. In contrast, NO_2^- showed reactivity in the presence of both mineral catalysts, and was stable in controls with 500 µM aqueous Fe^{2+}. The contrasting reactivity of the nitrogen oxides was also reflected in the solid phase Fe^{2+}/Fe^{3+} ratio determined at the end of the experiment (Fig. 2), revealing a trend of higher mineral oxidation with increasing NO_2^- concentration. Magnetite and GR showed disparate potential to produce N_2O. Concomitant with a more rapid NO_2^- consumption, N_2O production rates were more than 10 times higher when GR was the catalyst (Fig. 1B). At GR surface areas as observed for the Archean ocean analogue Lake Matano, Indonesia (~10^{-3} m^2 mL^{-1}, *23*, Fig. 1C), abiotic N_2O production rates were 25% (*low* NO_2^-) and >200% (*high* NO_2^-) the biotic production rates measured in modern oxygen minimum zones (~1 nM day^{-1}, *24*). As a reference, modern NO_2^- concentrations are near the bottom of the experimental range employed here, which extends higher to account for a range of possible Archean NO_x abundances (see below).

The conversion of NO_2^- to N_2O was not equimolarly balanced and we therefore considered accumulation of NO as intermediary species (*25*). After observing an initial modest NO accumulation, we injected concentrated hydrochloric acid in order to dissolve mineral particles and release any fraction bound to mineral surfaces (Fig. 1D). Indeed, the dissolution of mineral particles was followed by a spike in headspace NO concentration. At least 92% of the total amount of NO produced was bound to GR surfaces (97% was bound to magnetite surfaces). To rule out reaction of the acid itself with residual NO_2^-, we conducted controls with sulfuric acid and NO_2^- (table S2). Other controls to evaluate the stability of NO in the mineral suspension included acid injection at later time points in time-extended experiments observing NO yields at 220 hours (< 2.5 µM NO_2^-) similar to those at 50 hours after NO_2^- addition (table S2). We calculated the yield of NO in respect to the total added NO_2^- and, accordingly, 7% reacted to NO (over 63% that reacted to N_2O) with GR as catalyst and 69% reacted to NO (over 8% that reacted to N_2O) with magnetite as catalyst. The remaining product pool could be N_2 (*25*) and would only constitute a minor fraction of the total added nitrogen. Our data show that mineral-associated NO, presumably in the form of nitrosyl species (*26*), is a significant byproduct and geochemically stable in presence of Fe mineral phases.

Marine emissions accumulate atmospheric N_2O. To elucidate the impact of the experimentally derived production rates for the dispersion of N_2O in the seawater and emission to the Archean atmosphere, we combined diffusion models into a simple flux balance model (supplementary materials). We considered a 100 m deep slab of ocean beneath the photic zone as the part of the water column with a maximum overlap of NO_x^- ions from the surface and GR formation fueled by upwelling water rich in Fe^{2+} from the depth. An estimate of the GR particle concentration in the Archean ocean was informed by observed Fe particle numbers from seven modern marine and freshwater anoxic basins (supplementary materials), including the anoxic lake basin Kabuno Bay (KB) in East Africa (*27*). The peak Fe^{2+} concentration in the particulate fraction of KB anoxic waters (11 µM) closely reflects concentrations used for the thermodynamic modeling of GR precipitation in Archean seawater (*11*), which is why we used KB levels as a reference and enveloped that value with a putative lower and upper boundary of 50% and 500%. Archean seawater Fe^{2+} could have reached concentrations of 55 µM, as constrained by Fe^{2+}

toxicities on cyanobacteria (*28*) and the appearance of herringbone and micritic carbonates (*29*, *30*). At that upper boundary and under *low* NO_2^- conditions, net N_2O emissions conceivably reached 235 [98.1–413.9] nmol m^{-2} h^{-1} (95% CI, fig. S7, table S4), implicating 4 times the modern marine average flux (*31*). Overall, N_2O emissions from the ferruginous ocean gradually increased with the GR particle concentration in the water column.

To simulate the effect of N_2O fluxes triggered by mineral catalysis into an anoxic Archean atmosphere, we applied a photochemical model (*32*). We probed four different N_2O fluxes corresponding to *low* and *high* NO_2^- levels and Fe^{2+} concentrations in GR phases around the KB reference (table S4). Although the upper boundary of our estimates implicated near-modern N_2O abundances in the troposphere (0-13 km altitude, Fig. 3), N_2O concentration boundaries derived from *low* NO_2^- seawater levels and predicted to be 1-7 ppb are more realistic. This lower range is analogous to mixing ratios from Proterozoic atmosphere models assuming 1% of present oxygen levels (*5*, *8*). A striking difference is, however, the source of NO_x^- compounds, which was assumed to be microbial nitrification in the Proterozoic and abiotic nitrogen fixation prior to the GOE. Thus, abiotically derived NO_x^- can potentially produce tropospheric N_2O levels equal to those from biological origins.

Because of prevailing ferruginous conditions, the mineral reactions were likely limited by abiotic nitrogen fixation rates rather than mineral surface area. Previous seawater NO_x^- estimations – 8.7-24,000 µM (*16*), 1-10,000 µM (*20*), <1 µM (*17*) and 0.2-2 µM (*33*) – reveal a large uncertainty. For comparison, modern NO_2^- concentrations reach ~1.5 µM around oxygen minimum zones, but contrary to the Archean ocean, oxidoreductases effectively suppress NO_2^- accumulation (*34*). The associated nitrogen fixation rates differ between these studies. We carefully chose the initial NO_x concentrations in order to cover the lower end of the estimates, but also to demonstrate feasible reactions over at least two orders of magnitude in possible concentrations. Ongoing mineral reactions could further draw down NO_x concentrations, especially in proximity to particles, if consumption exceeded diffusion of new reactant. During active consumption, NO_x^- ions would diffuse from surface (0-40 m) and deeper (>140 m) water layers to mineral precipitates and replenish reactant. If mineral reactions indeed lowered local seawater NO_x^- concentrations, atmospheric N_2O may have reached sub-ppb concentrations, but not lower than HNO-derived N_2O concentrations (>0.5 ppb, Fig. 3). While the estimates from previous studies refer to the bulk seawater composition (values are average concentrations), top-down gradients of NO_x^- or conical zones of higher NO_x^- concentrations beneath rain out areas (Fig. 4) contributed perhaps to a more heterogeneous distribution. In such zones, NO_x^- may have reached concentrations well above the *low* NO_x^- range (1-5 µM) designated here, thus, justifying the inclusion of N_2O fluxes based on higher NO_x^- abundances.

The main sink of N_2O is photolysis by radiation < 230 nm (*35*) in the stratosphere, which governs the shape of the concentration profiles (Fig. 3). In the Archean atmosphere, N_2O abundances could have been higher due to i) additional sources and ii) protective agents against UV light. For instance, high-energy particles from solar flares led to N_2O formation most active at higher altitudes and could complement surface sources (*9*). These pathways played perhaps a more significant role in the Hadean or early Archean when the Sun was more active and the magnetic field openings were greater at the poles.

Furthermore, in the presence of methane hazes as proposed for the Archean, N_2O could have been shielded through strong UV absorption by fractal haze particles (*36*), which prolonged its lifetime. Both processes could have helped to stabilize atmospheric N_2O abundances that resulted from mineral-catalyzed N_2O production in the oceans.

Despite the tropospheric abundances predicted by our model, effects on the planetary climate were probably modest because N_2O would not be sufficiently concentrated to significantly increase the infrared atmospheric opacity in the CO_2 window regions. Especially in high CO_2 atmospheres, the N_2O radiative forcing is diminished since it may not occupy otherwise transparent infrared windows. The infrared window between 6 and 8 μm could potentially be filled by N_2O absorption, but this is dependent on atmospheric methane which absorbs at similar wavelengths (*8*). Since methane concentrations were likely > 100 ppmv (*37*), greenhouse warming by N_2O under our simulated conditions therefore contributed only weakly to a warmer climate under the faint young Sun of the Archean (*6*).

Effects of NO and N_2O on early anaerobic microbial life. It is plausible that as life co-evolved with the Earth system (*38*), it could have done so on a molecular level as an adaptation to abiotic NO and N_2O fluxes, too. Given GR phases at 100% KB equivalence, *low* seawater NO_2^- levels, and a 70% ocean cover of Earth's surface, N_2O emissions exported 10.4 Tg N yr^{-1} into the Archean atmosphere. Because of its high solubility, the fraction of N_2O dissolved in the ocean should not be underestimated. Under generally accepted Archean ocean conditions, N_2O reduction to N_2 is thermodynamically favorable. For example, coupled to H_2 oxidation (H_2 as a simple and available reductant), an affinity of up to 300 kcal per electron accepted by N_2O is significantly higher than that of any other redox reaction tested (fig. S8). Significant amounts of mineral surface-bound NO could have been transported down to the seafloor by settling of GR precipitates. Assuming a particle sinking velocity of 50 m day^{-1} (*39*), 1.2 Tg N yr^{-1} in the form of NO could have reached ocean sediments. This constitutes only ~1% of the downward NO_3^- flux (as comparable nitrogen oxide) measured above today's continental shelves (*40*). However, GR-shuttling of NO molecules may have been effective to reach benthic microbial life, where it then acted as a biological electron sink (*41*, Fig. 4). The availability of NO may have been essential for early denitrifying microorganisms because marine sediments in the Archean lacked nitrification as a source of nitrogen oxides. Conversely, NO could have also been damaging to microorganisms. The inhibitory effects of the NO molecule are well known and include production of radicals and the stimulation of nitrosative stress (*42*). In either case, NO exerted selective pressure and shaped the community composition. Based on enzymatic structural resemblance of NO and N_2O reductases (Nor and Nos) with cytochrome c oxidase (*5*, *43*, *44*) a primitive form of N_2O reduction likely preceded aerobic respiration. This concept is supported by a simple make-up of the respiratory chains involving quinone-dependent Nor and membrane-bound Nos, as present in some gram(+) bacteria (*4*, *45*). Evidently, the existence of NO and N_2O in the water column could have been feasibly exploited for the conversion of free energy and can at least explain biochemical patterns in modern respiratory enzyme complexes.

Conclusion

Our findings show that a significant portion of NO_x^- in the ferruginous Archean ocean was likely diverted to N_2O and NO leading to more oxidized products when compared to other sink pathways (ending in N_2 or ammonia). If this was the case, then the degree of thermodynamic disequilibria in the redox balance of the Archean nitrogen cycle may have been underestimated (*46*). Correspondingly, we caution to use N_2O as unique biosignature in exoplanet exploration. It is possible that conditions for the mineral-catalyzed N_2O production on early Earth-like exoplanets are even more favorable, resulting in N_2O atmospheric concentrations that could exceed modern ones (higher abiotic nitrogen fixation rates, higher Fe mineral load). Signals could be interpreted as false positives without any biological basis.

We present evidence that higher ozone levels may not be required to reach ppb N_2O concentrations prior to the GOE and lay out a concept of a complete abiotic N_2O cycle driven by mineral-catalyzed reactions (Fig. 4). Rather than being a mainly biological invention, the reduced branch of the abiotic nitrogen cycle was seemingly co-opted by early organisms. Even though the effects of abiotic N_2O production were probably modest on the early climate, marine sources of N_2O and NO could have markedly influenced the evolution of microbial respiration.

Materials and Methods

Mineral synthesis. Carbonate green rust was synthesized according to the following. In brief, 18.2 MΩ·cm water was made anoxic by boiling and sparging with CO_2/N_2 (20:80). An anoxic 0.4 M Fe^{2+}/Fe^{3+} solution (0.1 L) was prepared by mixing 7.42 g of $FeSO_4*7\ H_2O$ (>99%, Sigma Aldrich) and 2.66 g of anhydrous $Fe_2(SO_4)_3$ (97%, Sigma Aldrich). An alkaline, anoxic solution of 0.466 M Na_2CO_3 (Fisher Scientific) in 0.8 M NaOH (Fisher Scientific) (0.1 L) was prepared by dissolving NaOH first under a constant stream of CO_2/N_2 gas, after which Na_2CO_3 was added. Both solutions were stirred continuously at 500 rpm. The alkaline solution was injected into the Fe^{2+}/Fe^{3+} solution using CO_2/N_2 flushed syringes. Precipitation occurred immediately and the suspension was stirred in the dark for 24 hours. Magnetite was synthesized as nanoparticles following previously described protocols (*47*, *48*).

Mineral harvest. Green rust and magnetite precipitates were washed in an anaerobic chamber (0.5% H_2 in N_2, Coy Laboratory Products) using a vacuum filtration unit (Nalgene, Mfr # 130-4020) and 0.45 µm cellulose-acetate filter membranes (Sartorius). Anoxic 18.2 MΩ·cm water was poured onto the precipitates for a minimum of 8 cycles (pouring followed by extracting water). When filtrate flow ceased to a minimum, the wet mineral paste was removed from the filter. Wet carbonate green rust (73.8% water content) and wet magnetite (47.2% water content) were added to microcosms. The wet minerals were also used for mineralogical characterization (XRD and microscopy). For BET analysis, a defined amount of precipitate was dried in small boxes filled with drierite and placed into the anaerobic chamber. Dry weight was constant after 3-5 days.

X-ray diffractometry (XRD). Powder X-ray diffractometry was conducted on a subset of samples after synthesis and washing of the mineral products. A glycerol smear was prepared with 10 mg sample in the anaerobic chamber and sealed in a glass vial to prevent oxidation prior to analysis. To collect the XRD data, the sample was removed from the vial and spread across a quartz zero background plate that was placed onto a horizontal stage in a Bruker D-5000 diffractometer (Bruker, Germany) equipped with a Co Kα X-ray tube (30 kV, $\lambda = 1.791$Å). Signal peaks were compared to reference diffractograms in the RRUFF database. Instrument broadening was determined by a standard polycrystalline alumina sample. X-ray diffractometry data was analyzed with the CrystalDiffract software version 6.8.2 for Mac.

Scanning- and transmission-electron microscopy (SEM, TEM). Samples for SEM imaging were mounted on aluminum pin stubs with double-sided carbon tabs in the glove box and transported in a sealed jar with anoxic atmosphere to the microscope. Samples were not sputter-coated. Images were taken on an XL30 ESEM-FEG (Philips) operated at a 30 kV accelerating voltage and a 21 pA beam current. TEM samples were dispersed on a Lacey Carbon film using 200 mesh copper grids. The instrument used was a CM200 Field Emission Microscope at 200KV (Philips) with $C_s = 1.2$ mm and a PTP resolution of 0.25 nm. Imaging was done on a Gatan Orius CCD system.

Brunauer-Emmett-Teller (BET) surface area measurements. For analysis of the BET surface area, dried mineral precipitate was weighed inside the anaerobic chamber and added to a Florence glass flask that was closed with a rubber stoppers for transport to the instrument. BET surface in replicate samples (n = 3 for GR, n = 2 for magnetite) was quantified using N_2 gas on a Tristar II 3020 analyzer (Micromeritics Inc.). The instrument has a limit of detection of 1 m^2. Our results (table S1) are roughly consistent with previously determined BET values of 47 $m^2 g^{-1}$ for GR (*49*) and 95 $m^2 g^{-1}$ for magnetite (*50*).

We performed calculations of the mineral surface area for both minerals to supplement our measurements. To derive the mineral density, we calculated the average crystallite size by inserting the full width at half maximum, as determined from the diffractograms and the Bragg angle of the GR 0 0 3 reflection and of the magnetite 3 1 1 reflection, into the Scherrer equation. Mineral density was calculated using the formula $\rho = (M*Z)/(V_c*0.60225)$ where M is molar mass, Z is the number of molecules per crystallite and V_c is crystallite size. The density and the grain volume as measured by TEM/SEM were used to calculate the grain mass. The final value in $m^2 g^{-1}$ was derived from the grain mass and the grain surface area (TEM/SEM). For magnetite, we calculated a surface area of 88.8 $m^2 g^{-1}$. For green rust, we calculated a minimum approximation (surface of green rust sheets only) of 27.6 $m^2 g^{-1}$ and a maximum approximation (including surface between sheets) of 538.5 $m^2 g^{-1}$. Thus, our measured value for magnetite is somewhat lower than the calculated and literature value. The measured value for green rust is in good agreement with the literature value and at the lower end of the calculated range.

Incubation conditions. Interactions of nitrogen oxides with Fe minerals were tested in anoxic microcosms designed to mimic Archean ocean conditions as closely as possible. Borosilicate glass bottles (30-120 mL) were closed with thick butyl rubber stoppers and a headspace of 20% CO_2 in N_2 was used throughout the experiment. All glassware was washed with 2 M HCl prior to use. The liquid phase constituted one third of the microcosm total volume. We used a published recipe for artificial Archean seawater (*51*) and omitted any sulfur species. The pH was initially set to 7.3 using a CO_2–HCO_3^- buffer. We boiled 18.2 MΩ·cm water and sparged it with CO_2/N_2 (20:80) while it was cooling on ice. Salts were added during the sparging. The anoxic solution was then dispensed with a pipetor into microcosms in an anaerobic chamber (0.5% H_2 in N_2, Coy Laboratory Products). Nitrate and nitrite stock solutions were prepared with their respective sodium salts $NaNO_3$ (≥99%, Fisher Scientific) and $NaNO_2$ (≥97%, Acros Organics) and dissolved in artificial seawater. The solutions were then sparged with N_2 and filter-sterilized (0.8/0.2 µm pore seize, VWR) in the anaerobic chamber. Controls with aqueous Fe^{2+} were prepared in anoxic artificial seawater and $FeCl_2$ (≥99%, Fisher Scientific). Wet minerals were weighed in the anaerobic chamber and distributed into microcosms using ethanol-washed plastic spatulas. Prior to start of the incubations with the injection of the NO_x^- solution, mineral agglomerates were dissipated in an ultrasonic bath (Ultrasonic cleaner 2510, Branson Ultrasonics). Microcosms were shaken at 250 rpm in the dark and at room temperature over the whole duration of the experiment. Controls were incubated in the anaerobic chamber to test for potential leaking through stoppers, which did not occur. To dissolve mineral particles during incubations, 1.6 mL of concentrated 12N HCl or 37N H_2SO_4 was slowly injected through bottle septa to 10 mL mineral seawater-suspension. Dissolution of solid particles occurred instantly and the liquid first turned turbid orange-green and then clear green-yellow (HCl) or light yellow (H_2SO_4) within 15-20 hours. The last measurement of NO in the headspace was taken when the liquid was clear (fig. S5).

Dissolved nitrite, nitrate, ammonium, ferrous and ferric iron measurements. All dissolved analytes were quantified spectrometrically with plate assays. Nitrite in solution was quantified with the Griess reagent (Promega, Kit G2930). Nitrate was first reduced to nitrite by vanadium(III) chloride and then quantified as nitrite (*52*). Ammonium production was verified with the salicylic acid assay (*53*). To determine the Fe^{2+}/Fe^{3+} solid phase ratio, mineral particles were settled, after which supernatant artificial seawater was removed from the microcosms. Anoxic acidic extraction of green rust and magnetite was conducted as described previously (*47*). Ferrous and ferric ions in the extracts were measured by reaction with ferrozine after the method of Stookey (*54*).

N_2O gas measurements. To quantify N_2O production, 200 µL of headspace gas was sampled with a gas-tight syringe (VICI Precision Sampling) and injected onto a gas chromatograph (GC, SRI Instruments) equipped with an electron-capture detector (ECD). Two continuous HayeSep-D columns were kept at 90°C (oven temperature) and N_2 (UHP grade 99.999%, Praxair Inc.) was used as carrier gas. The ECD current was 250 mV and the ECD cell was kept at 350°C. The N_2O measurements were calibrated using customized standard mixtures (Scott Specialty Gases, accuracy ±5%) over a range of 0.25–100 ppmv. Gas accumulation in the microcosms was monitored over time. Gas concentrations were corrected using Henry's law and the dimensionless concentration constant $k_H^{cc}(N_2O) = 0.6112$ to account for gas partitioning into the aqueous phase at 25°C.

NO gas measurements. Nitric oxide (NO) was quantified in the microcosm headspace with a chemiluminescence-based analyzer (LMA-3D NO_2 analyzer, Unisearch Associates Inc.). Headspace gas (50 µL) was withdrawn with a CO_2-N_2-flushed gas-tight syringe and injected into the analyzer. The injection port was customized to fit the injection volume and consisted of a T-junction with an air filter at one and a septum at the other end. An internal pump generated consistent airflow. In short, sample NO was oxidized to NO_2 by a CrO_3 catalyst. The NO_2 flew across a fabric wick saturated with a Luminol solution. Luminol was obtained from Drummond Technology Inc. (Canada). Readings were corrected for background NO_2 every 15 minutes ("zeroing"). Shell airflow rate was kept at 500 mL min^{-1} and the span potentiometer was set to 8. Measurements were calibrated with a 0.1 ppm NO (in N_2) standard (<0.0005 ppm NO_2, Scott-Marin Inc.) over a range of 5–1,000 ppbv. Gas concentrations were corrected using Henry's law and the dimensionless concentration constant $k_H^{cc}(\mathrm{NO}) = 0.0465$ to account for gas partitioning into the aqueous phase at 25°C.

Diffusion modeling. The partial fluxes of the overall flux balance $\Phi_{sed} + \Phi_{par} = \Phi_{atm}$ were normalized to a 100 m vertical slab with 1 m^2 basis. The upper 100 m ocean water are typically considered as well-mixed, hence, reactant and catalyst are homogeneously distributed in that space. Depending on the water depth, a portion of the NO_x could reach the ocean floor, which is why we added a generic sediment flux (Φ_{sed}) to the balance equation. The dominant flux would emerge from floating GR mineral particles (Φ_{par}) that are distributed along the water column. For simplicity, we assume that all GR had aged into magnetite in the sediment and all floating particles were GR phases. We refer to the supplementary material for a more detailed description of the derivation of the partial fluxes, the error propagation method, and thermodynamic calculations.

Photochemical modeling. We have used an atmospheric photochemistry model to simulate the effects of N_2O emission into an anoxic atmosphere akin to the Archean Earth's condition. The photochemistry model used (*32*, *55*) has been validated by computing the atmospheric compositions of present-day Earth and Mars, as the outputs agreed with the observations of major trace gases in Earth's and Mars' atmospheres (*56*). For this work, we simulate a 1-bar atmosphere of 95% N_2 and 5% CO_2 to approximate the anoxic and CO_2-rich environment of the Archean Earth. We assume a surface temperature of 288 K and a stratospheric temperature of 200 K, and adopt the eddy diffusion coefficient derived from the number density profiles of trace gases on Earth (*57*). The photochemistry model includes a comprehensive reaction network for O, H, C, N, and S species including sulfur and sulfuric acid aerosols, and includes volcanic outgassing of CO, H_2, SO_2, and H_2S. The outgassing rate is not high enough to produce a H_2SO_4 aerosol layer in the atmosphere.

References and Notes

1. J. F. Kasting, Atmospheric composition of Hadean – early Archean Earth: The importance of CO. *Geological Society of America Special Papers*, 19–28 (2014).

2. S. Yoon *et al.*, Nitrous oxide reduction kinetics distinguish bacteria harboring clade I nosz from those harboring clade II NosZ. *Appl. Environ. Microbiol.* **82**, 3793–3800 (2016).

3. A. R. Babbin, D. Bianchi, A. Jayakumar, B. B. Ward, Rapid nitrous oxide cycling in the suboxic ocean. *Science*. **348**, 1127–1129 (2015).

4. J. Chen, M. Strous, Denitrification and aerobic respiration, hybrid electron transport chains and co-evolution. *Biochimica et Biophysica Acta (BBA) - Bioenergetics*. **1827**, 136–144 (2013).

5. C. L. Stanton *et al.*, Nitrous oxide from chemodenitrification: A possible missing link in the Proterozoic greenhouse and the evolution of aerobic respiration. *Geobiology*. **16**, 597–609 (2018).

6. D. O. Gough, in *Physics of Solar Variations* (Springer, Dordrecht, 1981), pp. 21–34.

7. L. V. Godfrey, P. G. Falkowski, The cycling and redox state of nitrogen in the Archaean ocean. *Nature Geoscience*. **2**, 725–729 (2009).

8. A. L. Roberson, J. Roadt, I. Halevy, J. F. Kasting, Greenhouse warming by nitrous oxide and methane in the Proterozoic Eon. *Geobiology*. **9**, 313–320 (2011).

9. V. S. Airapetian, A. Glocer, G. Gronoff, E. Hébrard, W. Danchi, Prebiotic chemistry and atmospheric warming of early Earth by an active young Sun. *Nature Geoscience*. **9**, 452–455 (2016).

10. S. W. Poulton, D. E. Canfield, Ferruginous conditions: A dominant feature of the ocean through Earth's history. *Elements*. **7**, 107–112 (2011).

11. I. Halevy, M. Alesker, E. M. Schuster, R. Popovitz-Biro, Y. Feldman, A key role for green rust in the Precambrian oceans and the genesis of iron formations. *Nature Geoscience*. **10**, 135–139 (2017).

12. J. Sorensen, L. Thorling, Stimulation by lepidocrocite (γ-FeOOH) of Fe(II)-dependent nitrite reduction. *Geochimica et Cosmochimica Acta*. **55**, 1289–1294 (1991).

13. H. Hansen, O. K. Borggaard, J. Sorensen, Evaluation of the free energy of formation of Fe(II)-Fe(III) hydroxide-sulphate (green rust) and its reduction of nitrite. *Geochimica et Cosmochimica Acta*. **58**, 2599–2608 (1994).

14. R. L. Mancinelli, C. P. McKay, The evolution of nitrogen cycling. *Orig Life Evol Biosph*. **18**, 311–325 (1988).

15. D. P. Summers, B. Khare, Nitrogen fixation on early Mars and other terrestrial planets: experimental demonstration of abiotic fixation reactions to nitrite and nitrate. *Astrobiology*. **7**, 333–341 (2007).

16. M. L. Wong, B. D. Charnay, P. Gao, Y. L. Yung, M. J. Russell, Nitrogen oxides in early Earth's atmosphere as electron acceptors for life's emergence. *Astrobiology*. **17**, 975–983 (2017).

17. S. Ranjan, Z. R. Todd, P. B. Rimmer, D. D. Sasselov, A. R. Babbin, Nitrogen oxide concentrations in natural waters on early Earth. *Geochemistry, Geophysics, Geosystems*. **20**, 2021–2039 (2019).

18. D. P. Summers, S. Chang, Prebiotic ammonia from reduction of nitrite by iron (II) on the early Earth. *Nature*. **365**, 630–633 (1993).

19. J. A. Brandes *et al.*, Abiotic nitrogen reduction on the early Earth. *Nature*. **395**, 365–367 (1998).

20. M. Laneuville, M. Kameya, H. J. Cleaves II, Earth without life: A systems model of a global abiotic nitrogen cycle. *Astrobiology*. **18**, 897–914 (2018).

21. I. Halevy, A. Bachan, The geologic history of seawater pH. *Science*. **355**, 1069–1071 (2017).

22. R. Buick, Did the Proterozoic "Canfield Ocean" cause a laughing gas greenhouse? *Geobiology*. **5**, 97–100 (2007).

23. A. Zegeye *et al.*, Green rust formation controls nutrient availability in a ferruginous water column. *Geology*. **40**, 599–602 (2012).

24. Q. Ji, A. R. Babbin, A. Jayakumar, S. Oleynik, B. B. Ward, Nitrous oxide production by nitrification and denitrification in the Eastern Tropical South Pacific oxygen minimum zone. *Geophysical Research Letters*. **42**, 10,755–10,764 (2015).

25. K. C. Grabb, C. Buchwald, C. M. Hansel, S. D. Wankel, A dual nitrite isotopic investigation of chemodenitrification by mineral-associated Fe(II) and its production of nitrous oxide. *Geochimica et Cosmochimica Acta*. **196**, 388–402 (2017).

26. A. D. Gordon *et al.*, Reduction of nitrite and nitrate on nano-dimensioned FeS. *Orig Life Evol Biosph*. **43**, 305–322 (2013).

27. M. Llirós *et al.*, Pelagic photoferrotrophy and iron cycling in a modern ferruginous basin. *Scientific Reports 2015 5*. **5**, 1–8 (2015).

28. E. D. Swanner *et al.*, Modulation of oxygen production in Archaean oceans by episodes of Fe(II) toxicity. *Nature Geoscience*. **8**, 126–130 (2015).

29. D. Y. Sumner, Carbonate precipitation and oxygen stratification in late Archean seawater as deduced from facies and stratigraphy of the Gamohaan and Frisco formations, Transvaal Supergroup, South Africa. *American Journal of Science*. **297**, 455–487 (1997).

30. D. Y. Sumner, J. P. Grotzinger, Were kinetics of Archean calcium carbonate precipitation related to oxygen concentration? *Geology*. **24**, 119 (1996).

31. G. Battaglia, F. Joos, Marine N_2O emissions from nitrification and denitrification constrained by modern observations and projected in multimillennial global warming simulations. *Global Biogeochemical Cycles*. **32**, 92–121 (2018).

32. R. Hu, S. Seager, W. Bains, Photochemistry in terrestrial exoplanet atmospheres. I. Photochemistry model and benchmark cases. *ApJ*. **761**, 1–29 (2012).

33. R. Hu, H. D. Diaz, Stability of nitrogen in planetary atmospheres in contact with liquid water. *ApJ*. **886**, 1–8 (2019).

34. M. A. Saito *et al.*, Abundant nitrite-oxidizing metalloenzymes in the mesopelagic zone of the tropical Pacific Ocean. *Nature Geoscience*. **13**, 355–362 (2020).

35. J. Kaiser, T. Röckmann, C. A. M. Brenninkmeijer, P. J. Crutzen, Wavelength dependence of isotope fractionation in N_2O photolysis. *Atmospheric Chemistry and Physics*. **3**, 303–313 (2003).

36. E. T. Wolf, O. B. Toon, Fractal organic hazes provided an ultraviolet shield for early Earth. *Science*. **328**, 1266–1268 (2010).

37. D. C. Catling, K. J. Zahnle, C. P. McKay, Biogenic methane, hydrogen escape, and the irreversible oxidation of early Earth. *Science*. **293**, 839–843 (2001).

38. L. E. Dietrich, M. M. Tice, D. K. Newman, The co-evolution of life and Earth. *Current Biology*. **16**, 395–400 (2006).

39. A. M. P. McDonnell, K. O. Buesseler, Variability in the average sinking velocity of marine particles. *Limnology and Oceanography*. **55**, 2085–2096 (2010).

40. A. H. Devol, Direct measurement of nitrogen gas fluxes from continental shelf sediments. *Nature*. **349**, 319–321 (1991).

41. A.-L. Ducluzeau *et al.*, Was nitric oxide the first deep electron sink? *Trends in Biochemical Sciences*. **34**, 9–15 (2009).

42. T. A. Heinrich *et al.*, Biological nitric oxide signalling: chemistry and terminology. *British Journal of Pharmacology*. **169**, 1417–1429 (2013).

43. M. Saraste, J. Castresana, Cytochrome oxidase evolved by tinkering with denitrification enzymes. *FEBS Letters*. **341**, 1–4 (1994).

44. A. Viebrock, W. G. Zumft, Molecular cloning, heterologous expression, and primary structure of the structural gene for the copper enzyme nitrous oxide reductase from denitrifying *Pseudomonas stutzeri*. *Journal of Bacteriology*. **170**, 4658–4668 (1988).

45. Suharti, S. de Vries, Membrane-bound denitrification in the gram-positive bacterium *Bacillus azotoformans*. *Biochemical Society Transactions*. **33**, 130–133 (2005).

46. J. Krissansen-Totton, S. Olson, D. C. Catling, Disequilibrium biosignatures over Earth history and implications for detecting exoplanet life. *Science Advances*. **4**, eaao5747 (2018).

47. J. M. Byrne *et al.*, Redox cycling of Fe(II) and Fe(III) in magnetite by Fe-metabolizing bacteria. *Science*. **347**, 1473–1476 (2015).

48. C. I. Pearce *et al.*, Synthesis and properties of titanomagnetite ($Fe_{3-x}Ti_xO_4$) nanoparticles: A tunable solid-state Fe(II/III) redox system. *Journal of Colloid and Interface Science*. **387**, 24–38 (2012).

49. A. G. B. Williams, M. M. Scherer, Kinetics of Cr(VI) reduction by carbonate green rust. *Environ. Sci. Technol.* **35**, 3488–3494 (2001).

50. Z. X. Sun, F. W. Su, W. Forsling, P.-O. Samskog, Surface characteristics of magnetite in aqueous suspension. *J of Colloid and interface science*. **197**, 151–159 (1998).

51. A. D. Anbar, A. D. Holland, The photochemistry of manganese and the origin of banded iron formations. *Geochimica et Cosmochimica Acta*. **56**, 2595–2603 (1992).

52. K. M. Miranda, M. G. Espey, D. A. Wink, A rapid, simple spectrophotometric method for simultaneous detection of nitrate and nitrite. *Nitric Oxide*. **5**, 62–71 (2001).

53. E. Kandeler, H. Gerber, Short-term assay of soil urease activity using colorimetric determination of ammonium. *Biol Fertil Soils*. **6**, 68–72 (1988).

54. L. L. Stookey, Ferrozine – a new spectrophotometric reagent for iron. *Anal. Chem.* **42**, 779–781 (1970).

55. R. Hu, S. Seager, W. Bains, Photochemistry in terrestrial exoplanet atmospheres. II. H_2S and SO_2 photochemistry in anoxic atmospheres. *ApJ*. **769**, 1–6 (2013).

56. R. Hu, thesis, Massachusetts Institute of Technology, Boston (2013).

57. S. T. Massie, D. M. Hunten, Stratospheric eddy diffusion coefficients from tracer data. *Journal of Geophysical Research: Atmospheres*. **86**, 9859–9868 (1981).

Acknowledgments:

General: We thank Melissa Kirven-Brooks and Chris McKay for their support during the initial experimental phase at the Ames Research Center. We are grateful to Karl Weiss, Sisouk Phrasavath, Emmanuel Soignard and Adam Smith for their help with the mineral analytics. We also thank Jaime Lopez for discussions on the diffusion modeling, and Ariel Anbar, Chadlin Ostrander, Jennifer Glass, Andreas Kappler, and Michael Russell for feedback on the manuscript.

Funding: Partial support to H.C.-Q. and S.B. was given by NASA’s Nexus for Exoplanet System Science (NExSS) research coordination network at ASU. S.B. and H.I. received critical funding to develop research through the NAI Early Career Collaboration Award. H.I. also received funding for this work from the NExSS grant NNX-15AQ73G.

Author contributions: S.B., H.I. and H.C.-Q. developed the experimental design. S.B. performed the experiments. S.B., T.E. and S.R. conducted thermodynamic and diffusion modeling. R.H. created the photochemical model. S.B. and H.C.-Q. drafted the manuscript. All authors participated in final revision of manuscript.

Competing interests: None to declare.

Data and materials availability: All data are available in the manuscript or the supplementary materials, and are available as raw data upon request from the authors.

Figures and Tables

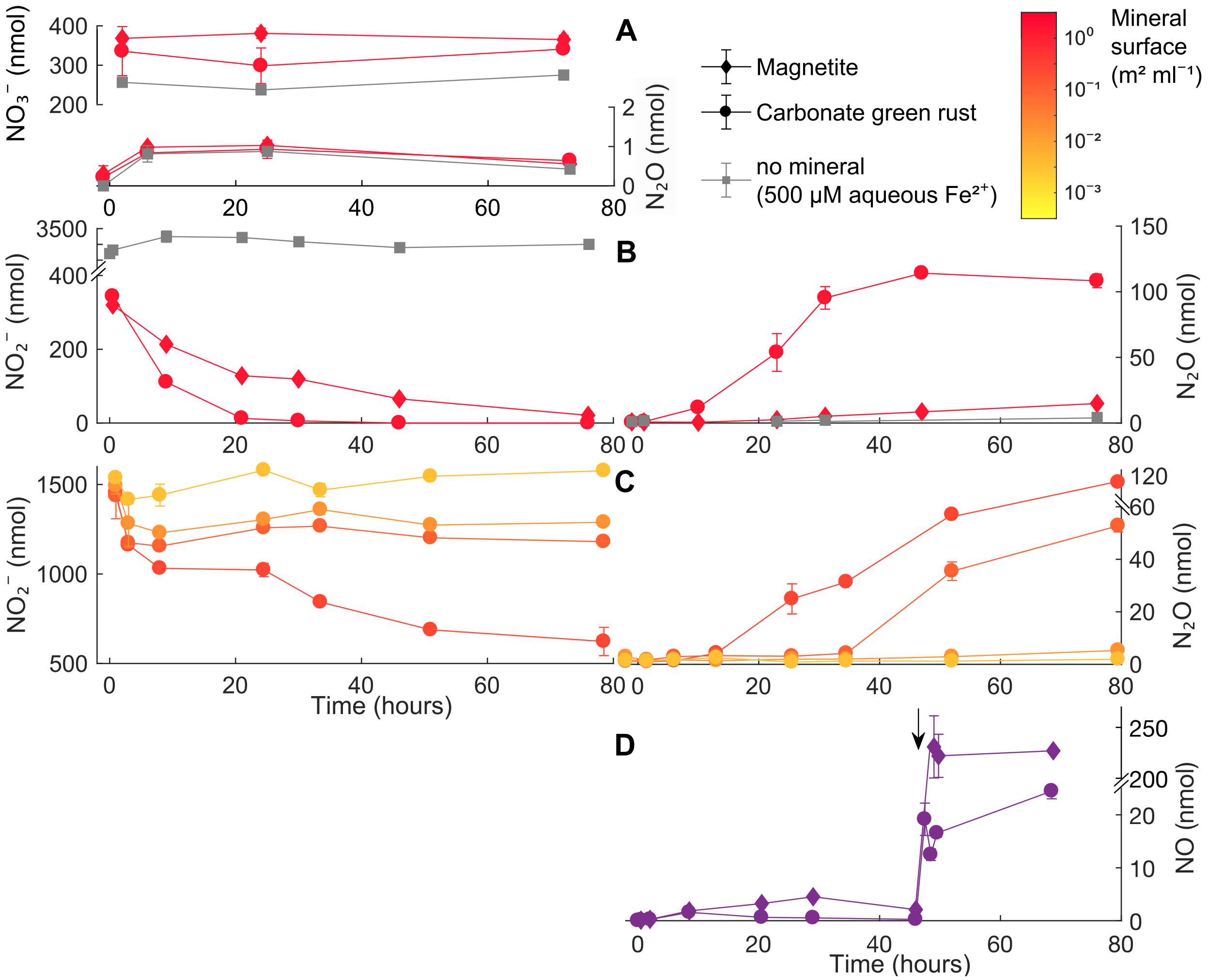

Fig. 1. Molecular NO_x^- consumption and associated NO and N_2O production with Fe minerals or aqueous Fe^{2+}. Dissolved NO_3^- and NO_2^- in anoxic artificial seawater solution were quantified concomitantly to NO and N_2O in the headspace. The results from incubations with initial NO_x^- concentrations in the *high* (20-35 μM) range are shown. The y-axes depict total quantities (gas + liquid phase) and are sometimes interrupted by breaks to better illustrate changes. (**A**) NO_3^- amended microcosms with GR and magnetite. (**B**) NO_2^- amended microcosms with GR and magnetite. (**C**) NO_2^- reduction and N_2O production under varying GR mineral surface area as controlled by the GR mass added. After an initial phase of rapid NO_2^- consumption, the reaction may become mineral surface-limited hindering the reduction of more NO_2^-. (**D**) NO formation during mineral incubations with 33 μM initial NO_2^-. The arrow indicates addition of concentrated hydrochloric acid resulting in subsequent mineral particle dissolution and outgassing of NO. Error bars denote one *SD* (n = 3).

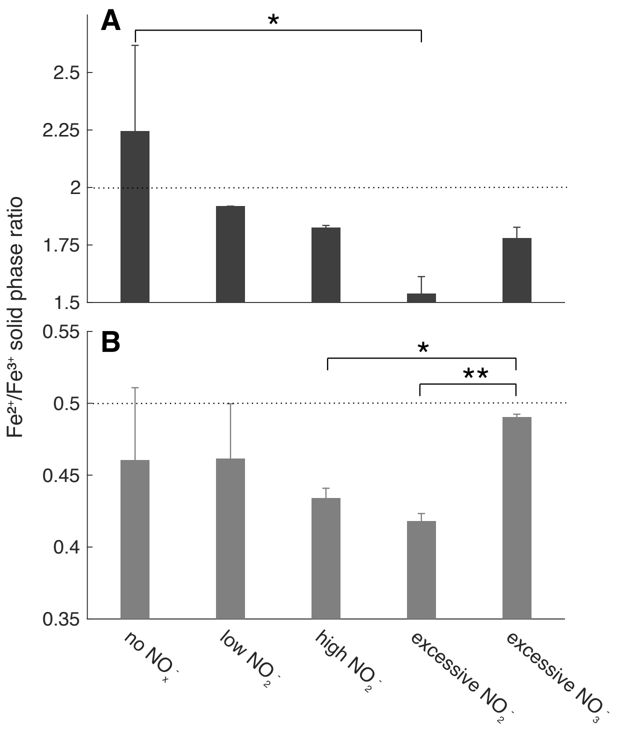

Fig. 2. Solid phase ratio of reduced and oxidized Fe in GR (A) and magnetite (B). Data were collected after acid digestion at the end of incubations. The dotted lines indicate stoichiometric GR and magnetite, respectively. For initial [NO$_x^-$], see Fig. 1 and table S3. *$P < 0.05$, **$P < 0.01$, Student's t test. Error bars denote one *SD* (n = 2-3).

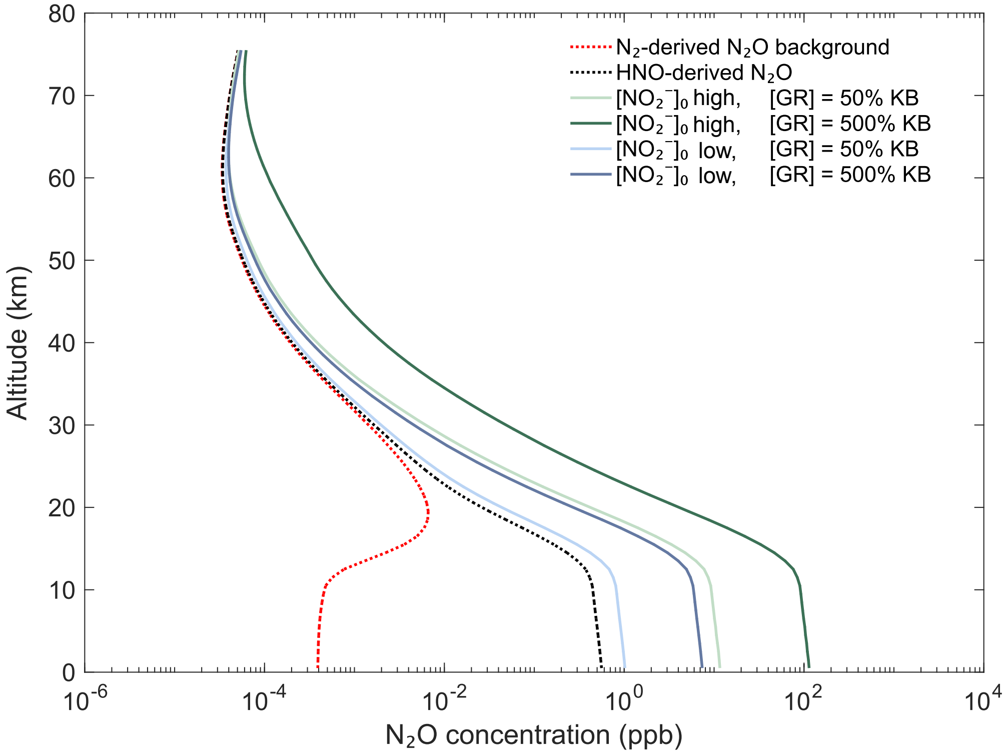

Fig. 3. Atmospheric N_2O abundances under influence of mineral-catalyzed N_2O production in the Archean ocean. Abundances are based on fluxes assuming GR phases in KB equivalents and *low* (blue) and *high* (green) seawater NO_2^- levels. The gray area marks the flux range potentially limited by NO_2^- supply (see text). Background N_2O formation occurred via the reaction $N_2 + O(^1D) + M \rightarrow N_2O + M$ and $O(^1D)$ was produced by photodissociation of CO_2 with photons more energetic than 167 nm. N_2O can also be derived directly through dehydrative dimerization of HNO that did not polymerize into NO_3^- or NO_2^- (*33*), but that contribution appeared to be minor. N_2O profiles based on mineral-catalyzed production do not account for N_2O from the HNO pathway.

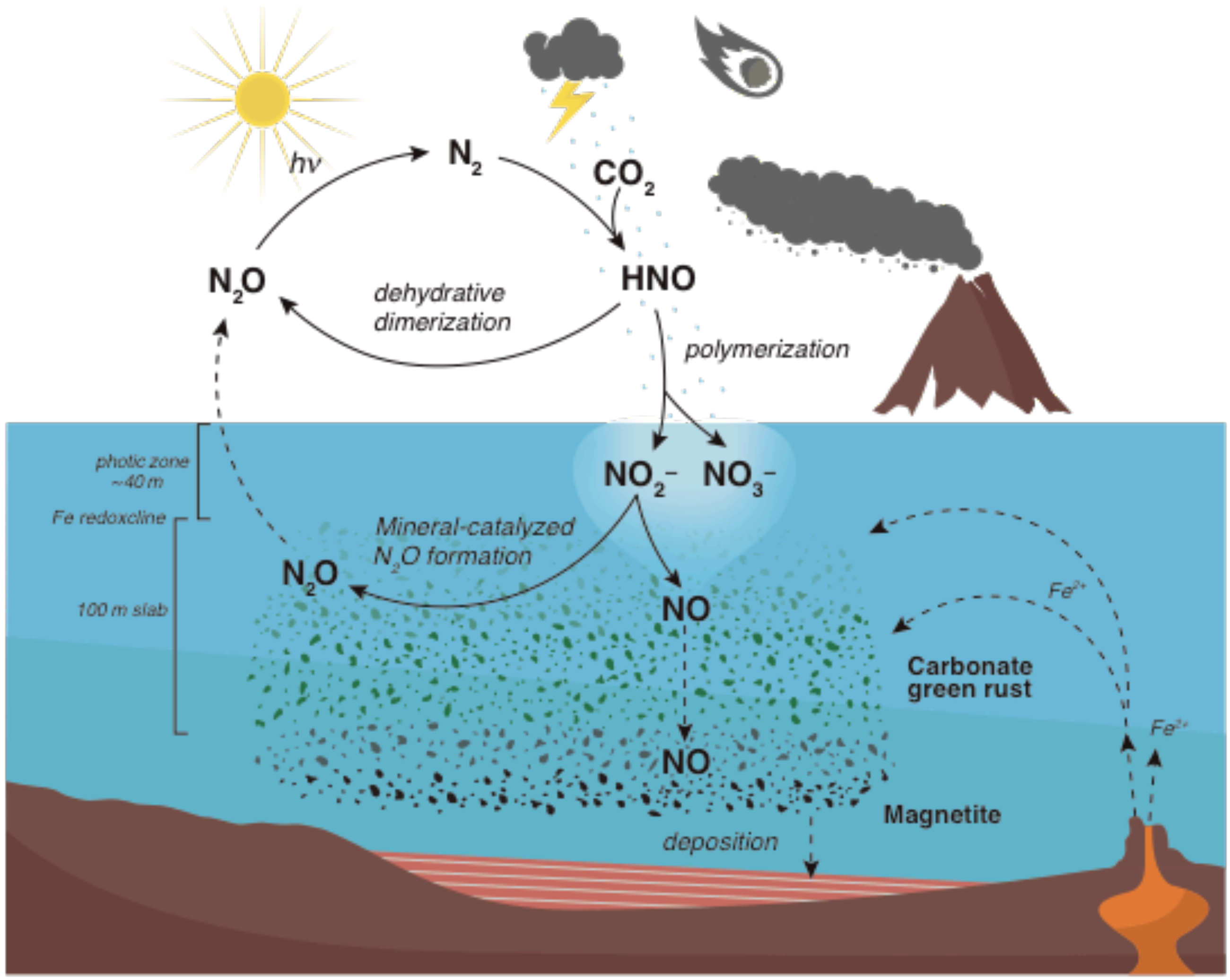

Fig. 4. Schematic depiction of mineral-catalyzed NO and N_2O formation at the junction of the early nitrogen and iron cycle. Heat shock reactions, such as stimulated by galactic cosmic rays, meteoritic impact plumes, volcanic and thunderstorm lightening, produced the central precursor HNO, which dimerized directly to N_2O or polymerized into NO_2^- and NO_3^- (*33*). These nitrogen oxides became interspersed into the surface ocean as plumes in the wake of distinct rain events and could have maintained average concentrations in surface seawater corresponding to levels used in our experiments. Any NO_3^- accumulated due to inefficient sinks. Upwelling Fe^{2+} precipitated into Fe oxyhydroxides and GR in the Fe redoxcline. Driven by Fe mineral phases, NO_2^- was reduced to N_2O. The abiotic nitrogen cycle was closed by photolytic destruction of emitted N_2O to N_2. As a byproduct, NO molecules remained bound at the mineral surface as nitrosyl. This way, GR may have served as NO shuttle enabling transport of nitrogen oxides into the deep ocean. Sinking GR particles transformed into magnetite, which then was deposited. Dashed lines mark diffusive or gravitational transport, whereas solid lines indicate chemical reactions.